

Enhancement of third-harmonic generation in a polymer-dispersed liquid-crystal grating

Przemyslaw P. Markowicz,^{a)} Vincent K. S. Hsiao, Hanifi Tiryaki, Alexander N. Cartwright, and Paras N. Prasad
The Institute for Lasers, Photonics and Biophotonics, Departments of Chemistry and Physics, University at Buffalo, State University of New York at Buffalo, Buffalo, New York 14260

Ksenia Dolgaleva, Nick N. Lepeshkin, and Robert W. Boyd
The Institute of Optics, University of Rochester, Rochester, New York 14627

(Received 7 December 2004; accepted 6 June 2005; published online 27 July 2005)

We report the observation of significant enhancement of one-step third-harmonic generation in a one-dimensional photonic crystal pumped by a near-infrared laser beam tuned to the low-frequency edge of the first photonic band gap. The third-harmonic phase matching can be controlled by changing the angle of incidence of the fundamental radiation, allowing tunability of the third-harmonic wavelength. The observed phenomenon was modeled theoretically using the transfer-matrix method. The enhancement is attributed to the combined action of phase-matching between the pump and harmonic waves and pump-field localization within the photonic crystal.
 © 2005 American Institute of Physics. [DOI: 10.1063/1.1999849]

Photonic crystals represent a class of materials in which alternating domains of high and low refractive indices produce an ordered structure with periodicity on the order of a wavelength of light. This new class of artificial periodic materials possesses unique optical properties.^{1–3} Recently there has been a great deal of interest in nonlinear photonic crystals,^{4–12} as they can allow enhancement of nonlinearity through their periodicity. Numerous experimental results on second-harmonic generation enhancement have been reported for various types of photonic crystals.^{7–9} Third-harmonic generation in one-dimensional (1D) photonic crystals via a two-step parametric process of second-harmonic generation and sum-frequency generation has been demonstrated experimentally.^{10,11} We recently demonstrated a dramatic enhancement of one-step phase-matched third-harmonic generation in a 3D polystyrene-air photonic crystal.¹² The peak of the THG enhancement occurred at the point where the third-harmonic wavelength approached the high-frequency edge of the photonic band gap.

In this letter we report on a significant enhancement of one-step third-harmonic generation in a 1D photonic crystal, with the fundamental wavelength tuned to the low-frequency edge of the first photonic band gap. The first experiments on third-harmonic generation in 1D periodic structures were conducted in cholesteric liquid crystals, which are helical birefringent structures, exhibiting only a weak periodic index modulation.^{13,14} Phase matching in these materials was achieved through temperature tuning of the pitch of the helical structure. Although the idea of phase-matched third-harmonic generation in layered structures was developed in the 1970's,¹⁵ diverse artificial periodically layered high-quality materials with strong index modulation were not available at that time. In particular, one- and two-dimensional periodic photonic structures became accessible only over past several years.

We observe enhancement of third-harmonic generation in a 1D liquid-crystal-polymer-composite holographic grat-

ing. The reflective grating for the present study was prepared in a way similar to that presented in Ref. 16. In our case a mixture of a photosensitive monomer (dipentaerythrol hydroxyl-penta-acrylate from Aldrich Chemical Co.), a liquid crystal (TL213; $n_o=1.527$, $n_e=1.766$, from EM Industries, Merck), and acetone (nonreactive solvent) was spin-coated on a glass substrate and illuminated by a 632 nm He-Ne laser beam in order to write the grating. The resulting structure, a 1D photonic crystal, was comprised of about 45 alternating low- and high-refractive-index layers, forming a 10 micron film on a glass substrate. The average index contrast between the high- and the low-index layers was of 0.15.

The measured transmission spectrum of the crystal is presented in Fig. 1 (solid lines). The minimum transmission of the structure is $\sim 15\%$ and the spectral FWHM of the band gap for normal incidence of light is ~ 90 nm. The losses on both sides of the photonic band gap are mainly caused by reflection from the crystal-air interface, as well as imperfections of the periodic structure.

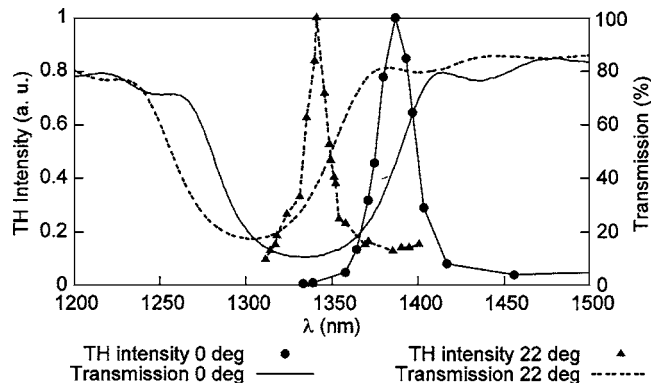


FIG. 1. Intensity of the third-harmonic signal generated from the 1D photonic crystal measured in transmission geometry as a function of the pump wavelength for normal and 22-degree-off-normal orientations of the photonic crystal (circles and triangles, respectively). The linear transmission spectra of the photonic crystal are shown to indicate the positions of the band edges (solid lines).

^{a)}Electronic mail: ppm@acsu.buffalo.edu

The pump beam for third-harmonic generation was produced by an optical parametric generator (OPG), pumped by a Clark-MXR CPA-2010 mode-locked Ti:sapphire oscillator-amplifier system, operating at a repetition rate of 1 kHz and generating 160 fs pulses at a wavelength of 775 nm. The third-harmonic signal was recorded as the wavelength of the OPG was tuned between 1.2 and 1.6 μm . The fundamental IR laser beam, generated by the OPG, was focused onto the photonic crystal. The third-harmonic light, generated within the crystal, was collected by a 10 \times objective with the numerical aperture of 0.25. The intensity at the focus was kept below 500 GW/cm² to avoid continuum generation from the sample.

When the incident pump beam was normal to the sample surface, the peak of THG occurred at a pump wavelength of 1.392 μm . As the crystal was tilted with respect to the pump beam, the maximum of the third-harmonic signal appeared at a shorter wavelength, depending on the angle of tilt. The reason for this behavior was that the location of the photonic band-gap position was shifted towards shorter wavelengths when the incident beam was off-normal. When the crystal was tilted 22° with respect to the normal orientation, the midgap position shifted from 1349 to 1302 nm. The peak of the third-harmonic signal followed the long-wavelength edge of the transmission gap and shifted from 1392 to 1340 nm. As confirmed below by our theoretical model, a major contribution to the enhancement is derived from phase matching. Figure 1 shows the wavelength dependence of the third-harmonic signal generated in the crystal for the normal and the 22°-off-normal illumination geometries (circles and triangles, respectively). The linear transmittance lines in Fig. 1 show that the maximum of the third-harmonic signal occurred when the fundamental wavelength was tuned close to the long-wavelength edge of the band gap. The third-harmonic radiation was ~ 7 –8 times more intense than that from a bulk material sample.

In order to theoretically analyze the experimental results, we developed a model based on the transfer-matrix technique^{17,18} which is frequently used for thin film characterization. The method is based on an exact solution of the Maxwell equations with boundary conditions applied at each interface of the sample. The advantages of this method are its simplicity and completeness with which it allows one to describe the propagation of light in a 1D periodic structure. Because of the space limitations, we do not present any mathematical details of the method in this letter.

Third-harmonic generation in each layer of the structure was included into the model by considering the layers as slabs of homogeneous material with a third-order nonlinearity, and applying the boundary conditions for the fundamental and the third-harmonic fields between the layers. In order to describe the third-harmonic generation in a layer of thickness L , we started from the driven wave equation:¹⁹

$$-\nabla^2 \tilde{E} + \frac{\varepsilon}{c^2} \frac{\partial^2 \tilde{E}}{\partial t^2} = -\frac{4\pi}{c^2} \frac{\partial^2 \tilde{P}^{\text{NL}}}{\partial t^2}. \quad (1)$$

Here \tilde{E} is the fundamental field, \tilde{P}^{NL} is the nonlinear polarization, giving rise to the third-harmonic field, c is the speed of light, and ε is the dielectric constant of the layer. Assuming that both the fundamental and the third-harmonic fields can be represented as plane waves, we can write

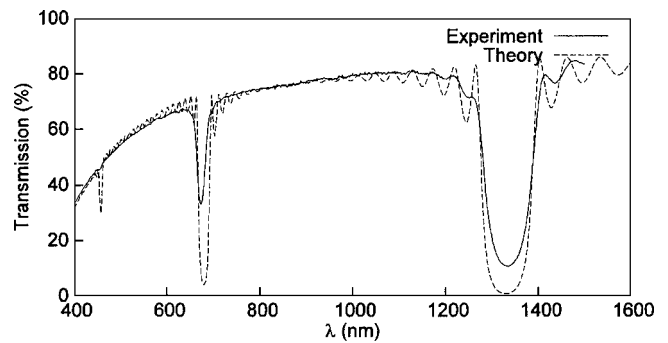


FIG. 2. Linear transmission at normal incidence as a function of wavelength, measured (solid line) and calculated (dashed line).

$$\tilde{E}_i(z, t) = A_i(z) \exp[i(k_i z - \omega_i t)] \quad (2)$$

and

$$\tilde{P}_3^{\text{NL}}(z, t) = \chi^{(3)} A_1^3 \exp[i(3k_1 z - \omega_3 t)], \quad (3)$$

where the index $i=1$ and 3 describes the fundamental and the third harmonic, respectively. $A_i(z)$ are the slowly varying functions of the coordinate z in the direction of the propagation. Substituting (2) and (3) into Eq. (1) and using the slow-amplitude approximation, we arrive at the equation

$$\frac{\partial A_3}{\partial z} = \frac{2\pi i}{c^2 k_3} \omega_3^2 \chi^{(3)} A_1^3 \exp[i(3k_1 - k_3)z] \quad (4)$$

for the third-harmonic electric-field amplitude $A_3(z)$. Neglecting z dependence of the electric-field amplitude of the fundamental wave within a single layer and using the undepleted-pump approximation, we can write the solution to Eq. (4) in the form

$$A_3(L) = \frac{2\pi\omega_3}{cn_3} \chi^{(3)} A_1^3 \frac{\exp[i(3k_1 - k_3)L] - 1}{3k_1 - k_3} + A_3(0). \quad (5)$$

The term $A_3(0)$ in the right part of the solution represents the third-harmonic radiation entering the layer. Equation (5) describes the third-harmonic radiation propagating in the positive z direction. A similar expression can be written for the third-harmonic generation propagating in the negative z direction. The above solution was included into the transfer matrices to obtain the third-harmonic intensity distribution within the 1D structure, as well as the intensity of the third-harmonic radiation, exiting the crystal in both positive and negative z directions.

To accurately model the optical properties of the sample, we used the experimentally measured parameters for the lattice constant a , the total number of layers, and the thickness of the sample. The refractive index dispersion was also measured, together with the index contrast between the higher- and the lower-index layers. By slightly varying the relative thicknesses of the higher- and the lower-index layers within the period, we obtained the transmission spectrum for the “virtual” sample, closely resembling the experimental data, as shown in Fig. 2. A linear absorption coefficient was extracted from the experimental data by fitting the measured transmission spectrum with a Lorentzian function. To account for this absorption, the calculated transmission was multiplied by the same Lorentzian function.

The third-harmonic generation was modeled with the parameters that gave us the best fit for the transmission spec-

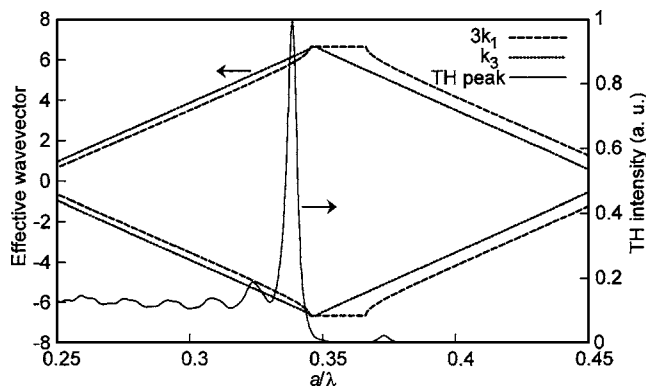


FIG. 3. Phase-matching condition described by means of the effective wave vectors plotted as functions of the normalized fundamental frequency ($3k_1$ is plotted with dashed lines, k_3 is plotted with dotted lines). Phase matching corresponds to the points of intersection of the curves. The theoretically calculated third-harmonic intensity is plotted with solid lines to display the position of its peak with respect to the phase-matching point.

trum. Phase matching between the fundamental and the TH waves in the structure was analyzed through calculation of their effective wave vectors. Figure 3 shows the real parts of the effective wave vectors $3k_1$ (dashed line) and k_3 (dotted line), corresponding to the fundamental and the third-harmonic waves, respectively, plotted as functions of the normalized fundamental frequency. The intersections of the $3k_1$ and k_3 curves are the points of phase matching between the fundamental and the third-harmonic waves. It can be seen from the graph that phase-matched third-harmonic generation should peak at the low-frequency edge of the first photonic band gap. We plot the intensity of the third-harmonic radiation generated by the sample on the same graph (solid line) to show that the third-harmonic intensity reaches its maximum when the THG phase-matching condition is satisfied. The position of the third-harmonic peak is slightly shifted towards lower frequencies with respect to the edge of the first photonic band gap. This may be due to a closely situated higher-order band gap in the region of the third harmonic, which does not let the TH peak occur for the values of the fundamental frequencies lying right at the edge of the first band gap.

Phase matching is not the only mechanism contributing to the experimentally observed third-harmonic peak. Another contribution to the third-harmonic enhancement is fundamental-field localization within the sample. Our calculations of the pump intensity distribution within the sample show that the highest local field inside the sample is 1.5 times stronger than the incident field; thus we estimate the maximum possible enhancement factor in THG due to this effect to be 3.4. Localization of the fundamental field can be understood in terms of the effective wave vector plot in Fig. 3. One can see that close to the band gap the slope of the k_1 -curve is large. In this region the group velocity of light decreases, leading to a high density of states and field localization. This local-field enhancement occurs at both the high- and low-energy edges of the band gap, whereas a third-harmonic peak is experimentally observed only at the position predicted by the phase matching consideration. In the numerical simulations shown in Fig. 3 the peak at the opposite side of the band gap does appear. However the THG

intensity at this peak is more than an order of magnitude weaker than that at the main peak where the phase matching is present. This comparison shows the relative contributions of the two effects responsible for the enhancement.

Third-harmonic generation conversion efficiency, defined as the ratio of the third-harmonic intensity to the fundamental intensity, was measured and calculated in both the transmission and reflection. The measured and calculated values of conversion efficiency were on the order of 10^{-8} . According to the measurements, third-harmonic was generated twice more efficient in transmission than in reflection. The calculations gave us a similar result.

In conclusion, we have demonstrated that a significant enhancement of third-harmonic generation can be achieved in a 1D photonic crystal when the fundamental wavelength approaches the low-energy edge of the first photonic band gap. The wavelength of the enhancement peak can be tuned by changing the crystal orientation and, hence, the band edge position. Our theoretical model predicts that the third-harmonic enhancement is due to both phase matching and pump-field localization within the structure. Thus, simple 1D photonic crystal structures can be designed to have a high efficiency of frequency conversion, and have a potential for becoming the basis for the next generation of nonlinear optical devices, where strong nonlinear material properties, phase matching, and field localization can be utilized simultaneously.

This work was supported at Buffalo by the Chemistry and Life Sciences Directorate of the Air Force Office of Scientific Research through a DURINT Grant No. F496200110358. The portion of the work performed at the University of Rochester was supported by ARO Grant DAAD19-01-1-0623.

¹P. N. Prasad, *Nanophotonics* (Wiley-Interscience, New York, 2004).

²J. D. Joannopoulos, R. D. Meade, and J. N. Winn, *Photonic Crystals: Molding the Flow of Light* (Princeton University Press, Princeton, NJ, 1995).

³M. Notomi, *Phys. Rev. B* **62**, 10696 (2000).

⁴*Nonlinear Photonic Crystals*, edited by R. E. Slusher and B. J. Eggleton (Springer, Berlin, 2003).

⁵R. S. Bennink, Y.-K. Yoon, and R. W. Boyd, *Opt. Lett.* **24**, 1416 (1999).

⁶P. Markowicz, C. Friend, Y. Shen, J. Swiatkiewicz, P. N. Prasad, O. Toader, S. John, and R. W. Boyd, *Opt. Lett.* **27**, 351 (2002).

⁷M. Scalora, M. J. Bloemer, A. S. Manka, J. P. Dowling, C. M. Bowden, R. Viswanathan, and J. W. Haus, *Phys. Rev. A* **56**, 3166 (1997).

⁸G. D'Aguzzo, M. Centini, M. Scalora, C. Sibilia, Y. Dumeige, P. Vidakovic, J. A. Levenson, M. J. Bloemer, C. M. Bowden, J. W. Haus, and M. Bertolotti, *Phys. Rev. E* **64**, 016609 (2001).

⁹J. Martorell, R. Vilaseca, and R. Corbalan, *Appl. Phys. Lett.* **70**, 702 (1997).

¹⁰S. Zhu, Y. Zhu, and N. Ming, *Science* **278**, 843 (1997).

¹¹Y. B. Chen, C. Zhang, Y. Y. Zhu, S. N. Zhu, H. T. Wang, and N. B. Ming, *Appl. Phys. Lett.* **78**, 577 (2001).

¹²P. P. Markowicz, H. Tiryaki, H. Pudavar, P. N. Prasad, N. N. Lepeshkin, and R. W. Boyd, *Phys. Rev. Lett.* **92**, 83903 (2004).

¹³J. W. Shelton and Y. R. Shen, *Phys. Rev. Lett.* **25**, 23 (1970).

¹⁴J. W. Shelton and Y. R. Shen, *Phys. Rev. A* **5**, 1867 (1972).

¹⁵N. Bloembergen and A. J. Sievers, *Appl. Phys. Lett.* **17**, 483 (1970).

¹⁶V. K. S. Hsiao, T. C. Lin, G. S. He, A. N. Cartwright, P. N. Prasad, L. V. Natarajam, V. P. Tondiglia, and T. J. Bunning, *Appl. Phys. Lett.* **86**, 131113 (2005).

¹⁷J. E. Sipe, *J. Opt. Soc. Am. B* **4**, 481 (1987).

¹⁸D. S. Bethune, *J. Opt. Soc. Am. B* **6**, 910 (1989).

¹⁹R. Boyd, *Nonlinear Optics* (Academic, New York, 1992).